Supporting Information

Plasma-Induced Large-Area N,Pt-Doping and Phase Engineering of MoS$_2$ Nanosheets for Alkaline Hydrogen Evolution

Yan Sun,[+a] Yipeng Zang,[+c] Wenzhi Tian,[a] Xujiang Yu,[a] Jizhen Qi,[d] Liwei Chen,[a,b,d] Xi Liu,*[b] and Huibin Qiu*[a]

[a.] Department State Key Laboratory of Metal Matrix Composites, Frontiers Science Centre for Transformative Molecules, School of Chemistry and Chemical Engineering, Shanghai Jiao Tong University, Shanghai 200240, P. R. China E-mail: hbqiu@sjtu.edu.cn.

[b.] In-situ Centre for Physical Science, School of Chemistry and Chemical Engineering, Shanghai Jiao Tong University, Shanghai 200240, P. R. China Email: liuxi@sjtu.edu.cn.

[c.] State Key Laboratory of Catalysis, Dalian National Laboratory for Clean Energy, Dalian Institute of Chemical Physics, Chinese Academy of Sciences, Dalian 116023, P. R. China

[d.] CAS Centre for Excellence in Nanoscience Suzhou Institute of Nano-Tech and Nano-Bionics (SINANO), Chinese Academy of Sciences, Suzhou, 215123, P. R. China

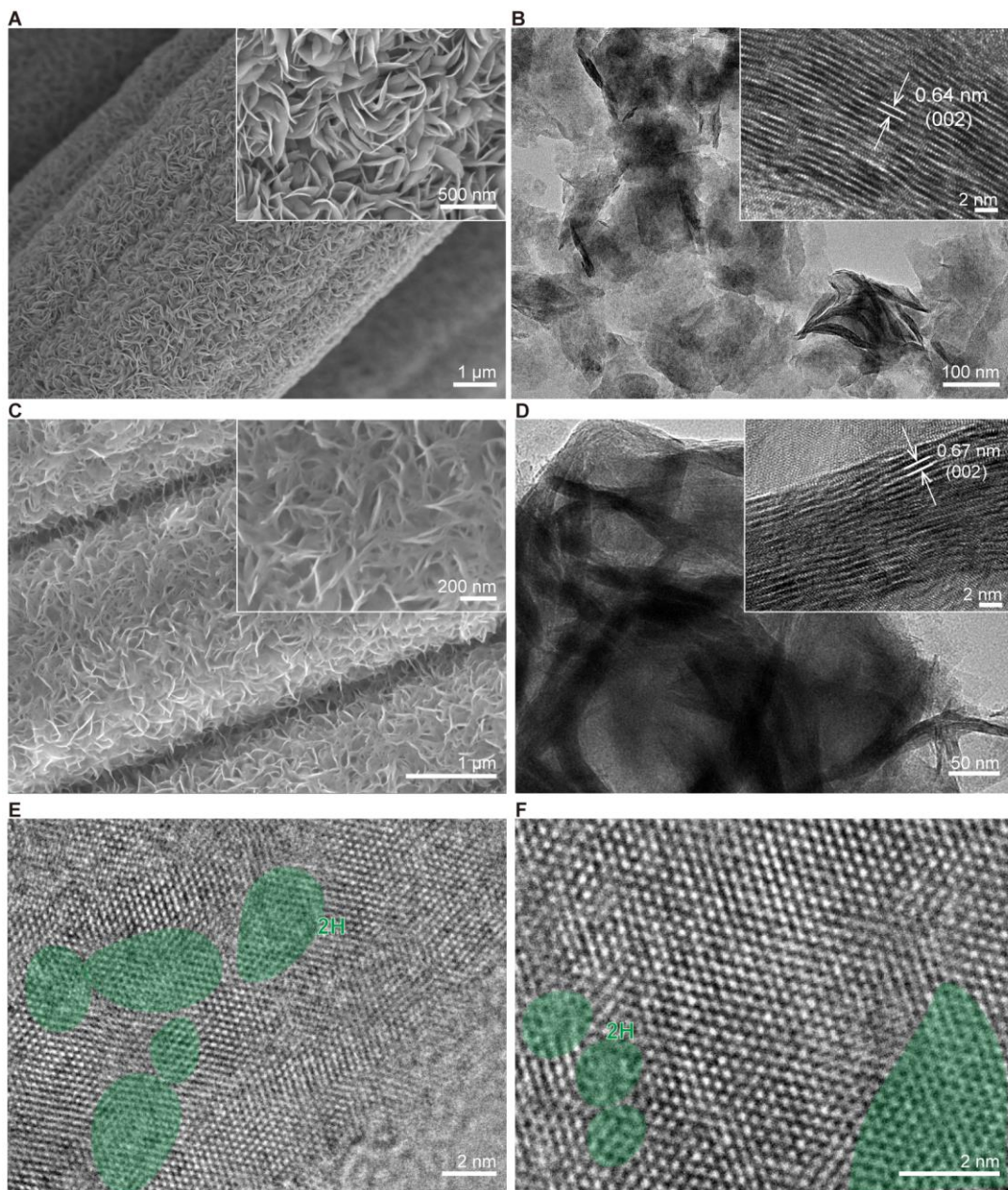[+] These authors contributed equally to this work

Figure S1. (A) SEM and (B) TEM images of MoS_2 nanosheets synthesized directly on CCs through a hydrothermal method. The interlayer distance (0.64 nm) corresponds to the 2H phase of MoS_2. (C) SEM, (D) TEM and (E, F) HRTEM images of MoS_2 nanosheets treated in N_2 plasma for 2 h.
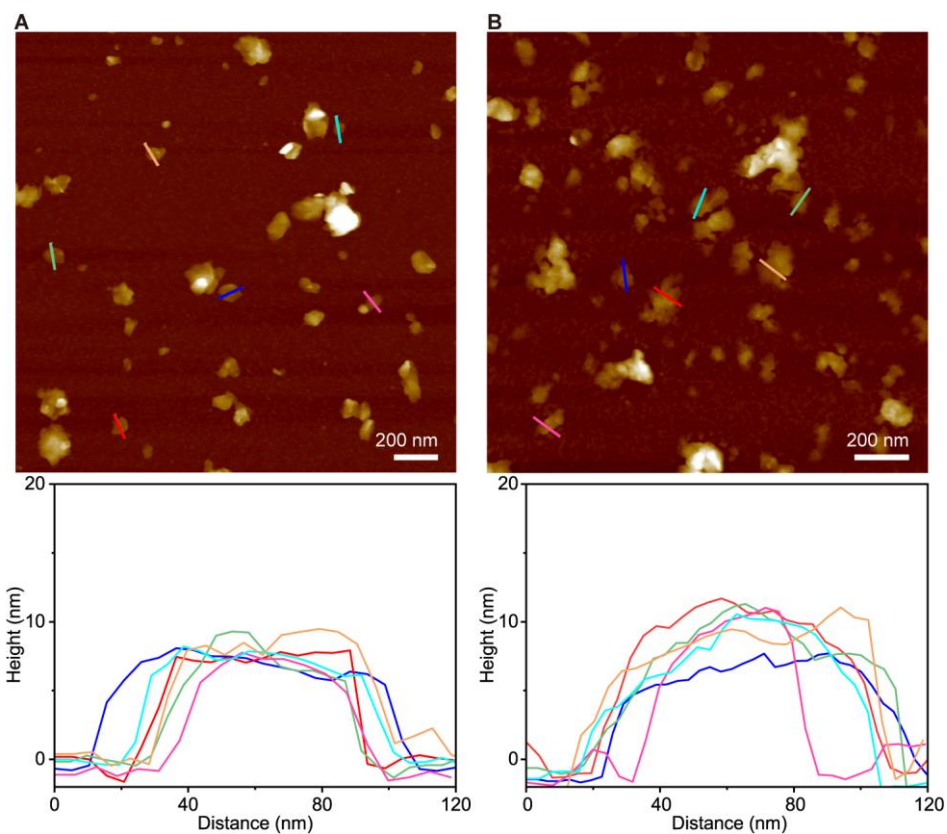
Figure S2. AFM height images and corresponding height profiles of (A) N-MoS$_2$ and (B) N,Pt-MoS$_2$ nanosheets. The samples were sonicated in ethanol and then the resulting dispersions were drop-casted on silicon wafers for AFM analysis.
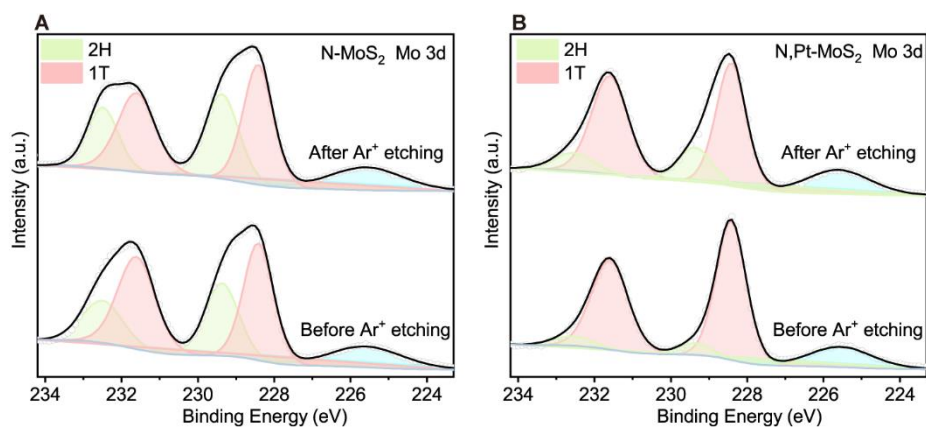

Figure S3. XPS spectra of Mo 3d for (A) N-MoS$_2$ and (B) N,Pt-MoS$_2$ nanosheets before and after Ar$^+$ etching for 1 h under photon energy of 1486.6 eV.
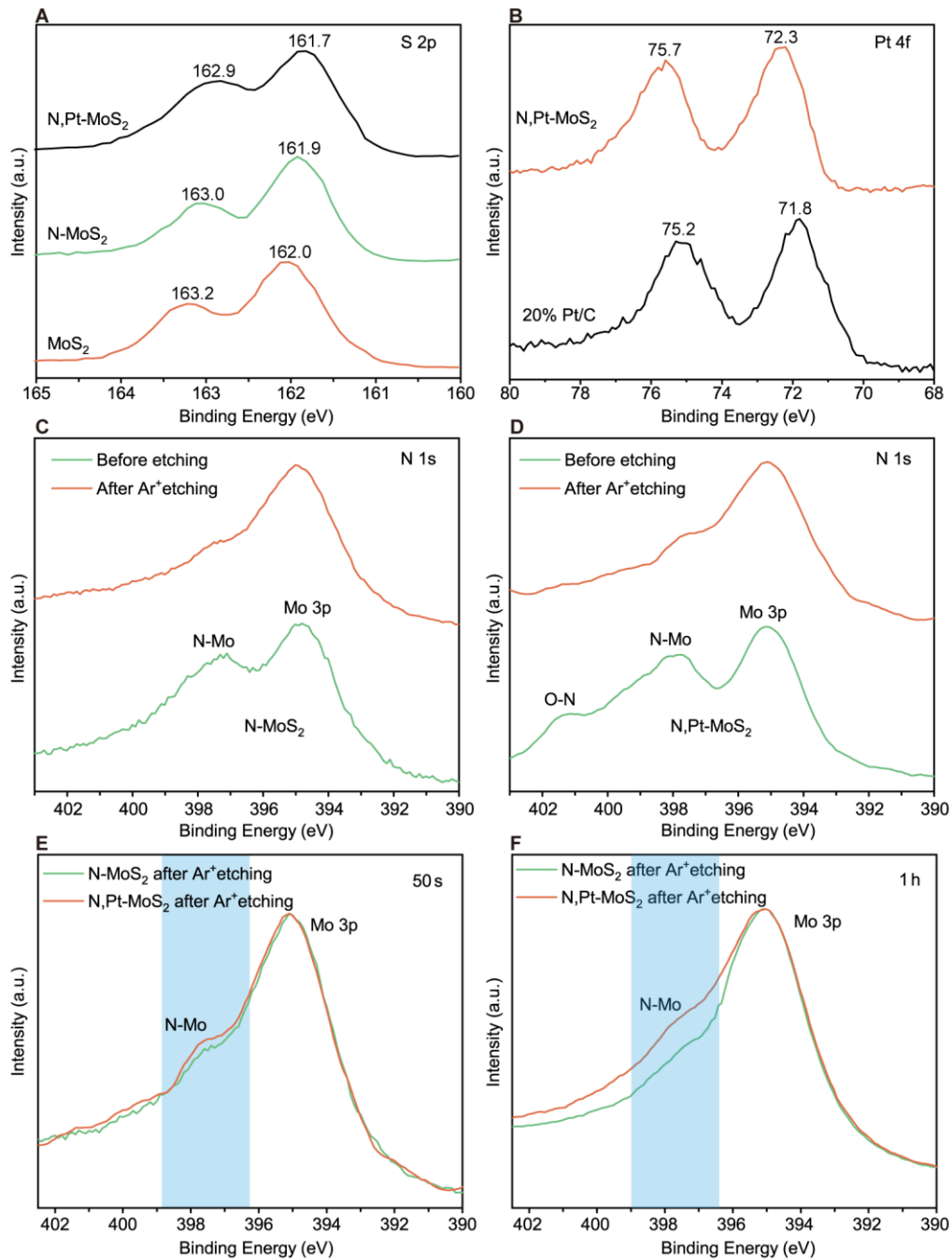
Figure S4. (A and B) XPS spectra of (A) S 2p and (B) Pt 4f for MoS_2, N-MoS_2, and N,Pt-MoS_2 nanosheets. (C and D) XPS spectra of N 1s for N-MoS_2 and N,Pt-MoS_2 nanosheets before and after Ar^+ etching for 50 s under photon energies (1486.6 eV). (E and F) XPS spectra of N 1s for N-MoS_2 and N,Pt-MoS_2 nanosheets before and after Ar^+ etching for 50 s and 1 h.
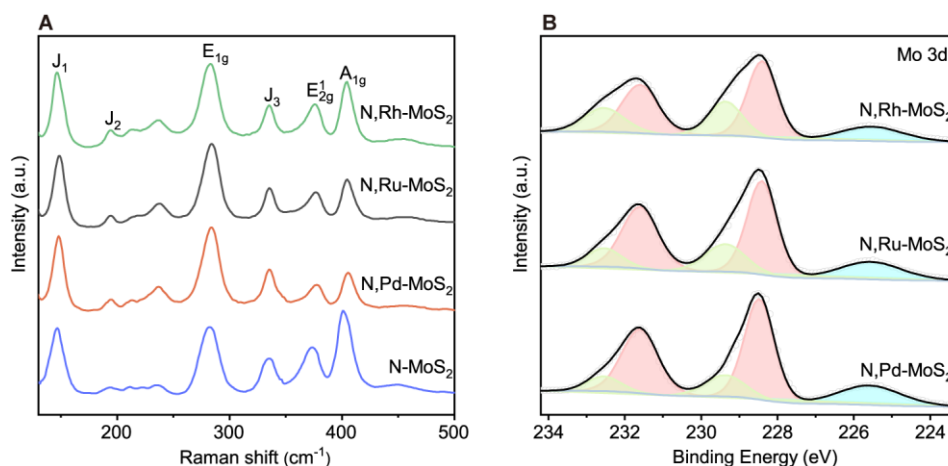
Figure S5. (A) Raman and (B) XPS spectrta of Mo 3d for N,Rh-MoS$_2$, N,Ru-MoS$_2$, and N,Pd-MoS$_2$ nanosheets.

Table S1. Electrochemical performances comparison of N,Pt-MoS$_2$ nanosheets with the ever-reported MoS$_2$-based catalysts in alkaline condition.

electrocatalyst	Electrolyte	Overpotential at 10 mA cm^{-2} (mV)	Tafel slop (mV dec^{-1})	Reference
N,Pt-MoS$_2$	1.0 M KOH	38	39	This work
1T-MoS$_2$/NiS$_2$	1.0 M KOH	116	72	#1
Co-MoS$_2$	1.0 M KOH	48	52	#2
N,Mn-MoS$_2$	1.0 M KOH	66	50	#3
1T-MoS$_2$/CoS$_2$	1.0 M KOH	71	60	#4
1T-MoS$_2$	1.0 M KOH	250	67	#5
Fe-MoS$_2$/CoMo$_2$S$_4$	1.0 M KOH	122	90	#6
MoS$_2$-NiS$_2$/N-graphen	1.0 M KOH	172	70	#7
Ru-MoS$_2$	1.0 M KOH	41	114	#8
MoS$_2$/Co$_9$S$_8$/Ni$_3$S$_2$/Ni	1.0 M KOH	113	85	#9

Table S2. Electrochemical performances comparison of N,Pt-MoS$_2$ nanosheets and previously reported Pt-based catalysts.

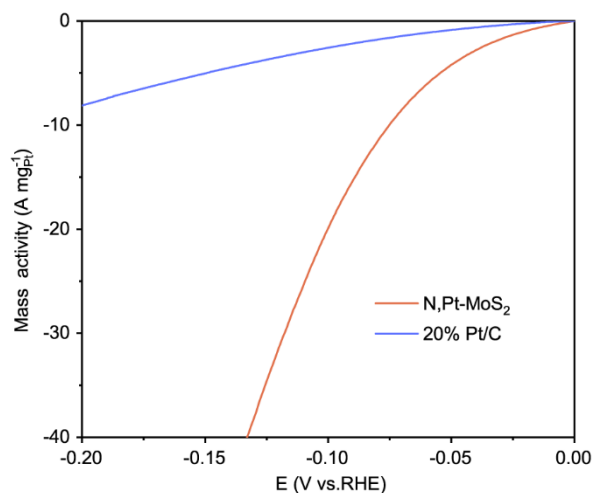| Electrocatalyst	Electrolyte	Overpotential at 10 mA cm^{-2} (mV)	Tafel slop (mV dec^{-1})	Reference
N,Pt-MoS$_2$	1.0 M KOH	38	39	This work
Pt/Fe$_5$Ni$_4$S$_8$	1.0 M KOH	65	44	#10
PtNi-O/C	0.1 M KOH	40	79	#11
MoO$_x$/Pt	1.0 M KOH	-	54	#12
Ni-MOF@Pt	1.0 M KOH	102	88	#13
PtNi NWs/C	1.0 M KOH	40	-	#14
Pt/Ni(HCO$_3$)$_2$	1.0 M KOH	44	45	#15
Pt-MoS$_2$	0.5 M H$_2$SO$_4$	50	40	#16
Pt@PCM	0.5 M H$_2$SO$_4$	105	63	#17
Pt SA/m-WO$_{3-x}$	0.5 M H$_2$SO$_4$	38	45	#18
Pt-MoS$_2$	0.1 M H$_2$SO$_4$	~150	96	#19

Figure S6. Mass activity of Pt atoms of N,Pt-MoS$_2$ nanosheets in comparison with 20% Pt/C catalyst for HER.
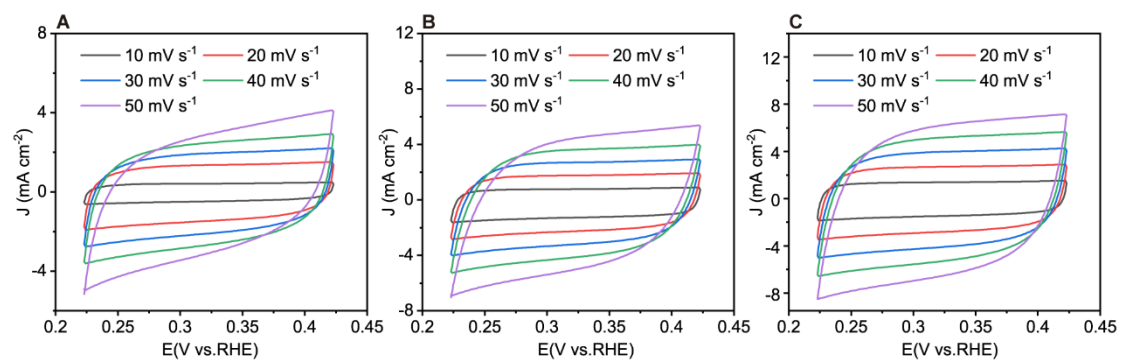

Figure S7. CV curves at different various scan rates of (A)MoS$_2$, (B)N-MoS$_2$, and (C) N,Pt-MoS$_2$ nanosheets in 1.0 M KOH solution at the potential range of 0.223 to 0.423 V (*vs.* RHE).
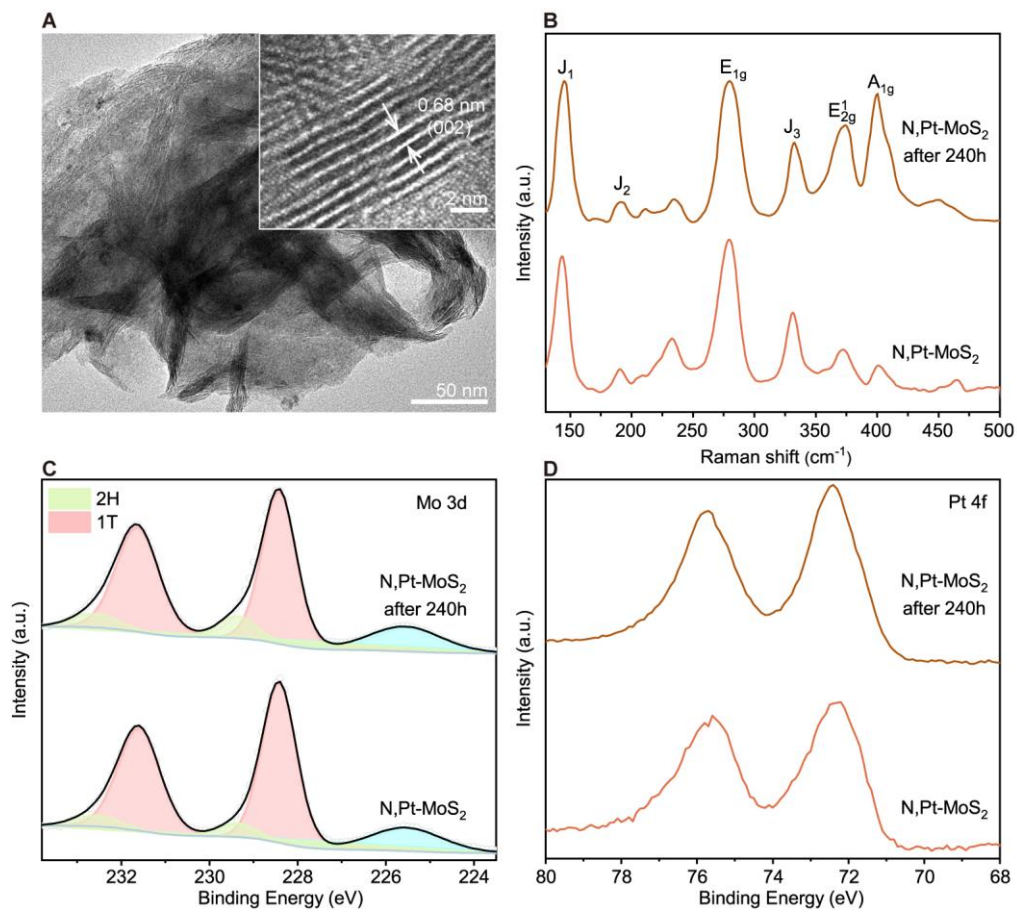
Figure S8. (A) TEM images, (B) Raman spectra, XPS spectra of (C) Mo 3d and (D) Pt 4f for N,Pt-MoS$_2$ nanosheets after cycling 240 h.
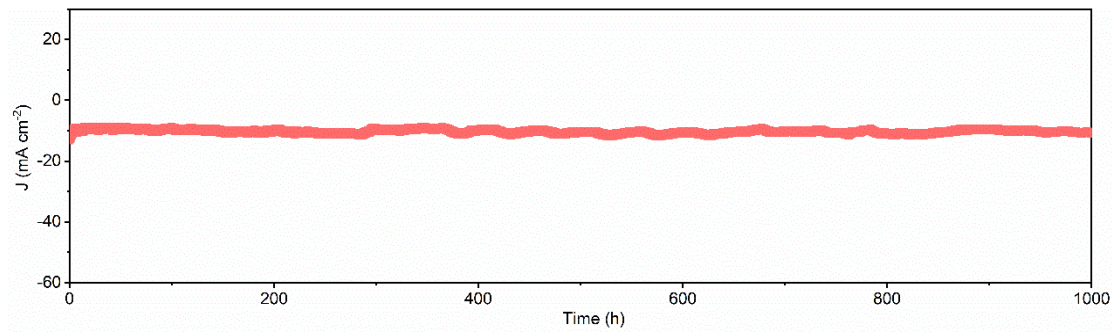
Figure S9. Chronopotentiometry measurement of N,Pt-MoS$_2$ nanosheets at a current density of 10 mA cm^{-2} in 1.0 M KOH aqueous solution for a continuous period of 1000 h.
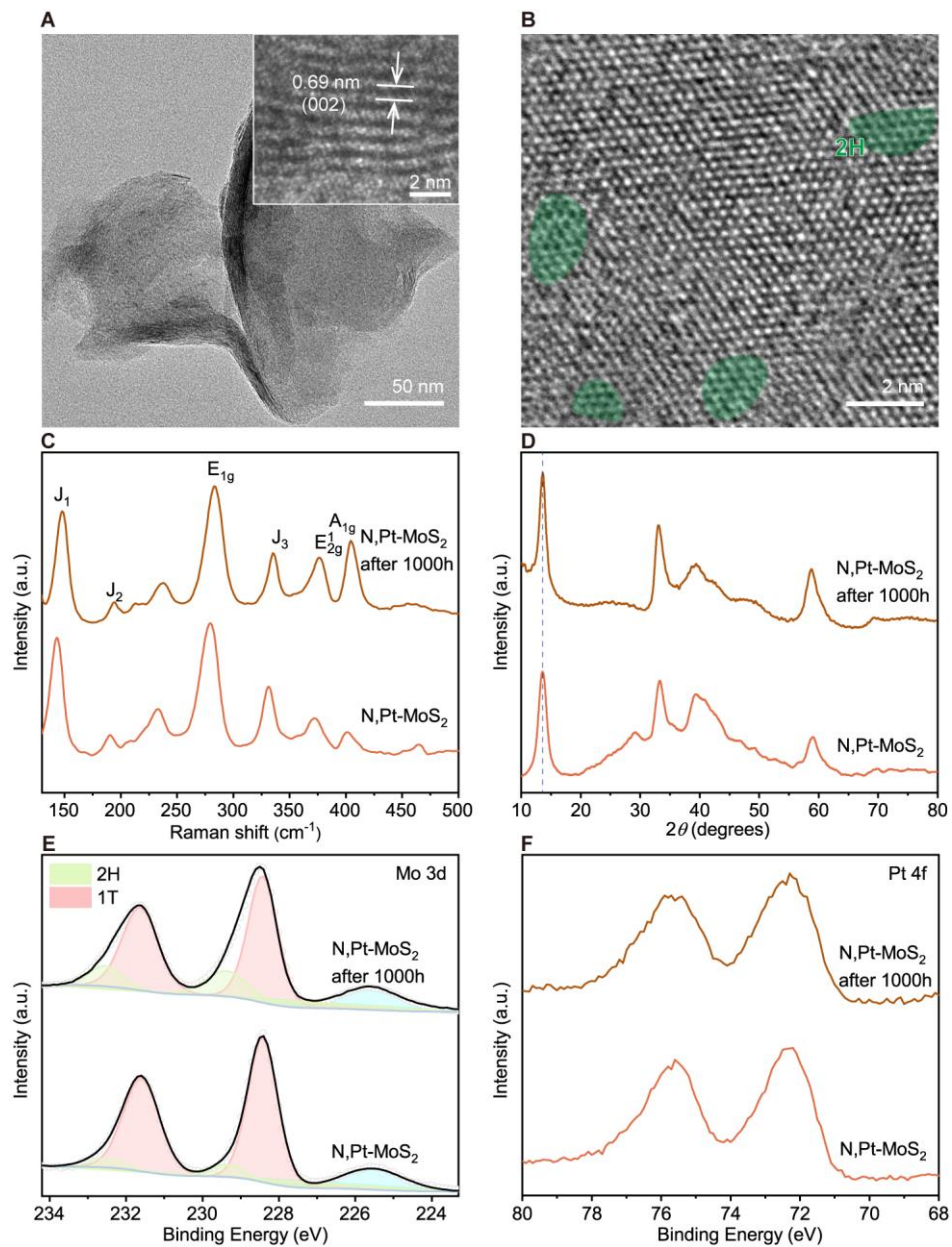

Figure S10. (A) TEM, (B) HRTEM images, (C) Raman spectra, (D) XRD and XPS spectra of (E) Mo 3d and (F) Pt 4f for N,Pt-MoS$_2$ nanosheets after cycling 1000 h.

The N,Pt-MoS$_2$ nanosheets may have three possible lattice structures (Figure S11). Amongst, lattice I possessed the lowest formation energy (Table S3) and was consequently adopted for further calculation.
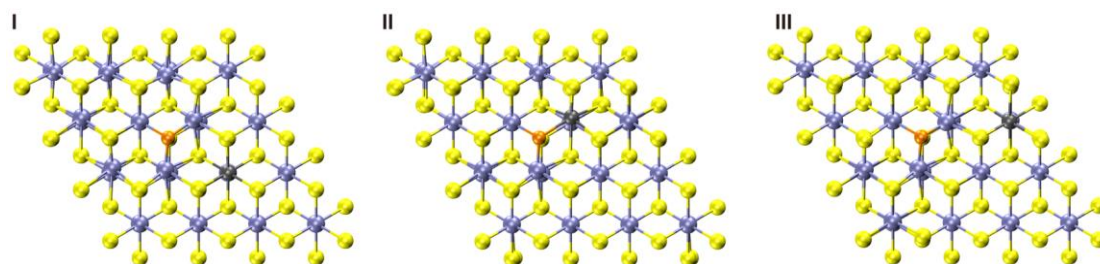

Figure S11. Three possible lattice structures of N,Pt-MoS$_2$ nanosheets.

Table S3. Formation energy of different lattice structures of N,Pt-MoS$_2$ nanosheets.

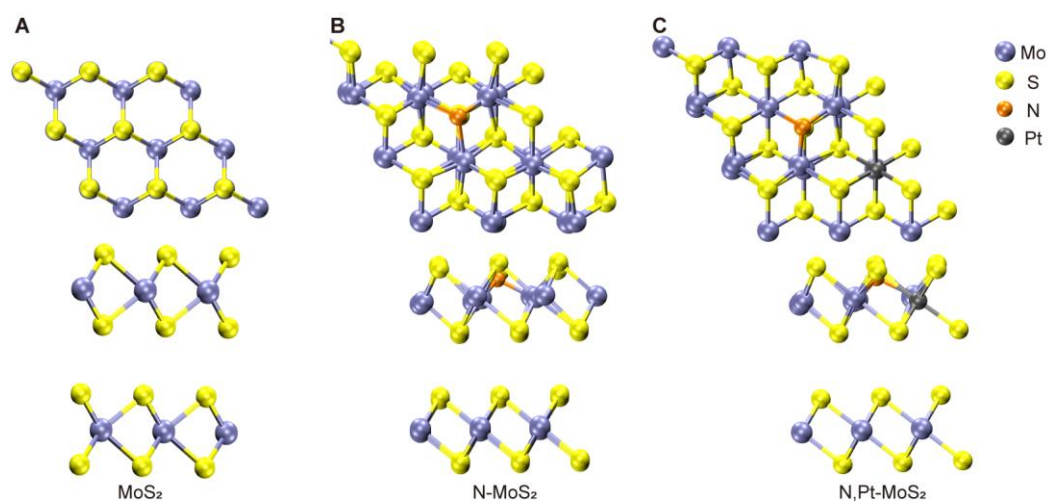| Structures	I	II	III
Formation energy (eV)	-582.01	-581.40	-581.67

Figure S12. Optimized atomic configurations of top-view and side-view structures of (A) MoS$_2$, (B) N-MoS$_2$ and (C) N,Pt-MoS$_2$ nanosheets.
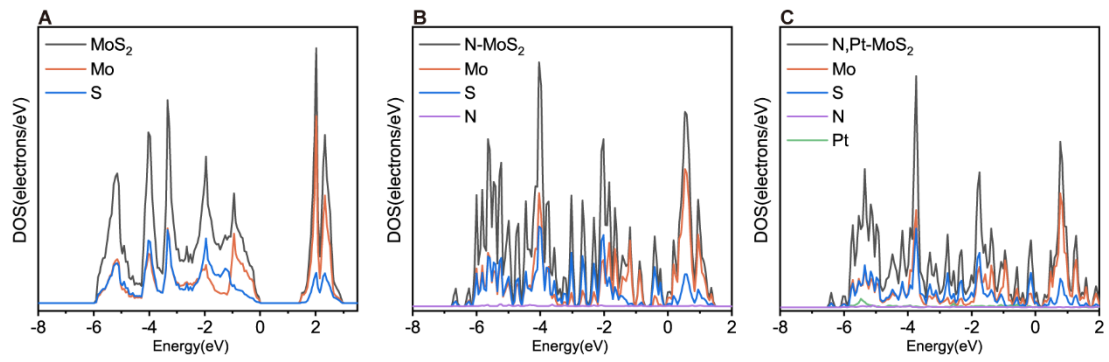
Figure S13. PDOS distribution of (A) MoS$_2$, (B) N-MoS$_2$, and (C) N,Pt-MoS$_2$ nanosheets.
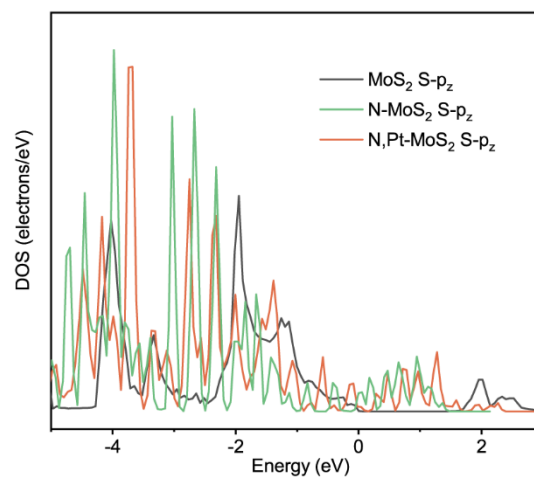

Figure S14. PDOS distribution of S atoms in MoS$_2$, N-MoS$_2$, and N,Pt-MoS$_2$ nanosheets.

We compared water absorption on different sites of the N-MoS$_2$ nanosheets (Figure S15). Water absorption on S site near the N dopant revealed the most negative energy (I, Table S4) and was consequently adopted for further calculation.
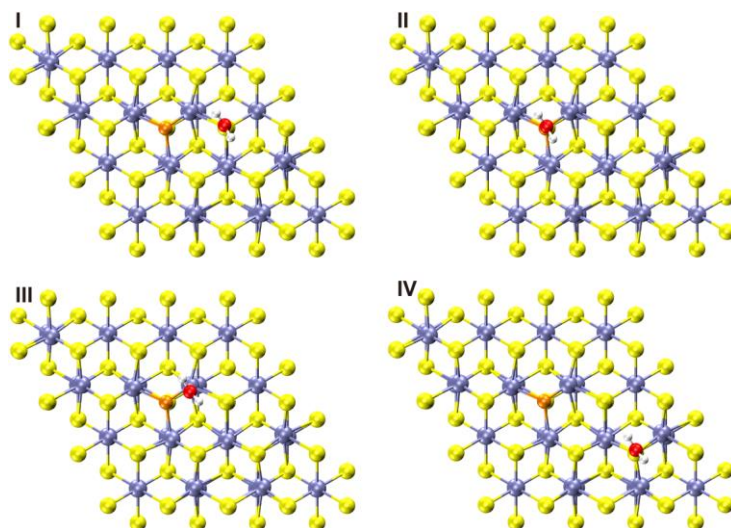

Figure 15. Water adsorption on different sites of N-MoS$_2$ nanosheets.

Table S4. Energy of water adsorption on different sites of N-MoS$_2$ nanosheets.

Sites	I	II	III	IV
Water adsorption energy (eV)	-1.39	-0.98	-0.80	-1.30

In order to reveal the actual active sites, we compared the energies of water absorption and dissociation on a series of possible active sites of the N,Pt-MoS$_2$ nanosheets. Based on the atomic configurations of the N,Pt-MoS$_2$ nanosheets, six different sites for water absorption were considered (Figure S16). Amongst, water absorption on S site between N and Pt atoms (Figure S16I) possessed the most negative energy (Table S5) and was consequently adopted for further water absorption calculation. Meanwhile, since water dissociation is a rate-determine step for HER, we also compared the relative energy diagram along the reaction coordinate on different active sites of the N,Pt-MoS$_2$ nanosheets (Figure S18). Amongst, S site between N and Pt atoms (Figure S17I) also possessed lowest water dissociation energy (Table S6) and was therefore chosen S as the actual active sites.
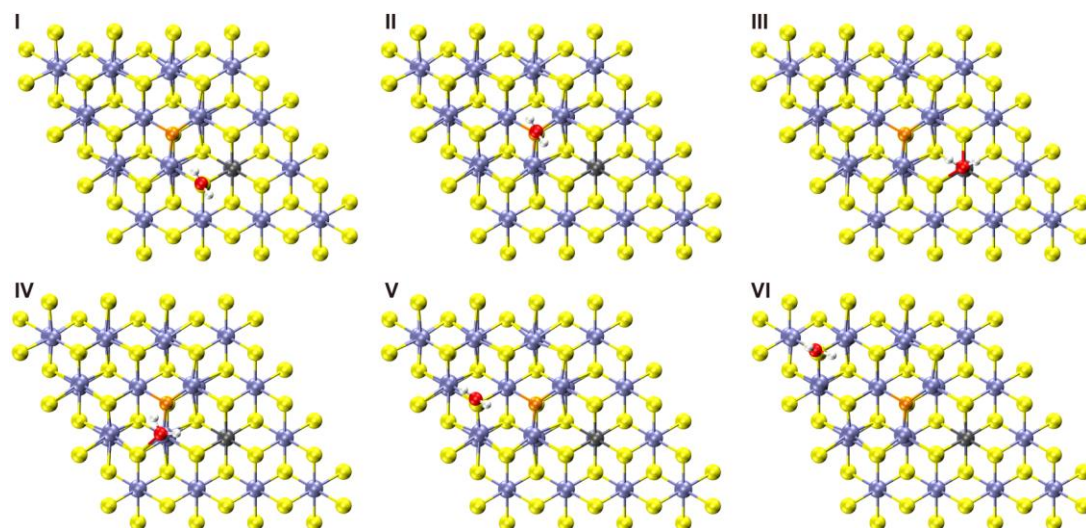

Figure S16. Water adsorption on different sites of N,Pt-MoS$_2$ nanosheets.

Table S5. Energy of water adsorption on different sites of N,Pt-MoS$_2$ nanosheets.

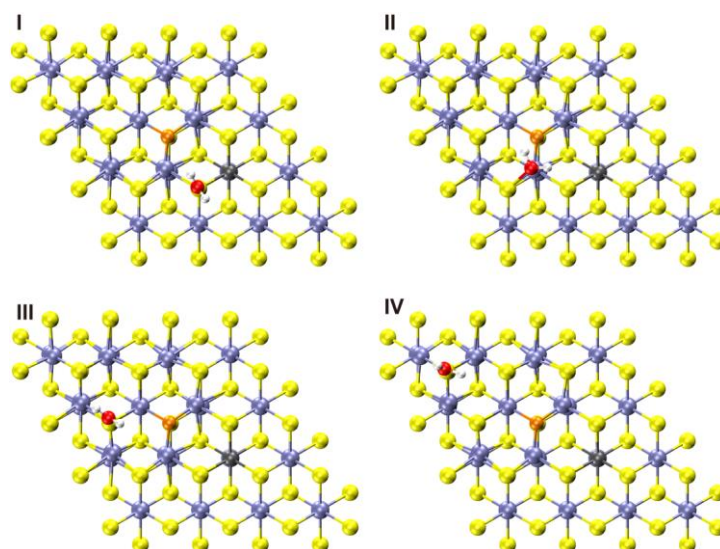| Sites	I	II	III	IV	V	VI
Water adsorption energy (eV)	-1.71	-0.89	-1.43	-0.59	-1.04	-1.30

Figure S17. Water adsorption on different sites of N,Pt-MoS$_2$ nanosheets.
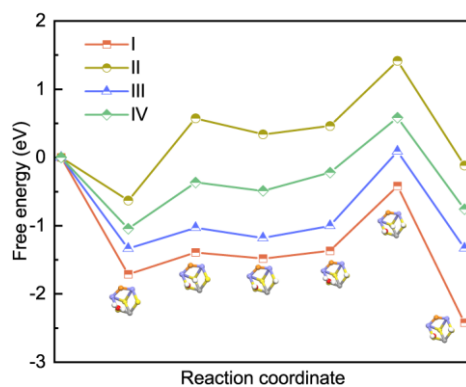
Figure S18. Relative energy diagram along the reaction coordinate on different sites of N,Pt-MoS$_2$ nanosheets in Figure S17.

Table S6. Max energy barrier for water dissociation from different sites of N,Pt-MoS$_2$ nanosheets.

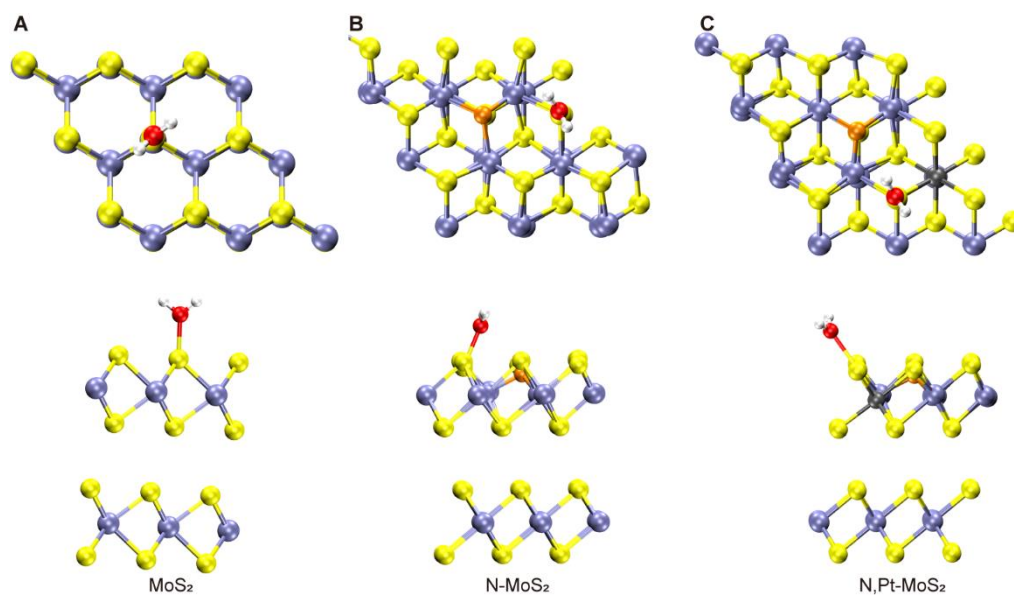| Sites	I	II	III	IV
Max water dissociation energy barrier (eV)	0.95	1.20	1.11	1.06

Figure S19. Optimized top-view and side-view structures of (A) MoS$_2$, (B) N-MoS$_2$, and (C) N,Pt-MoS$_2$ nanosheets with water adsorbed on the surface.
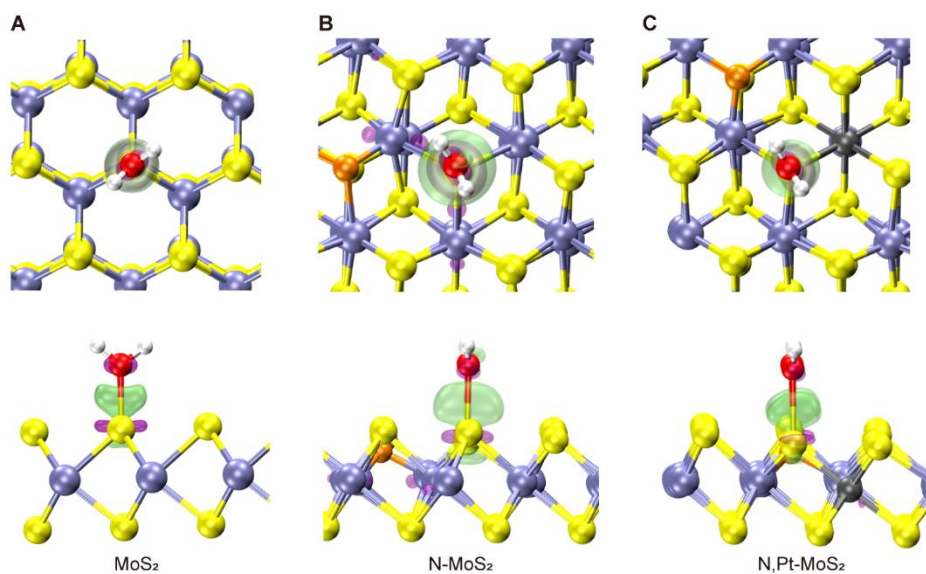
Figure S20. Top and side view of electron density difference with water molecules adsorbed on (A) MoS_2, (B) N-MoS_2, and (C) N,Pt-MoS_2 nanosheets.
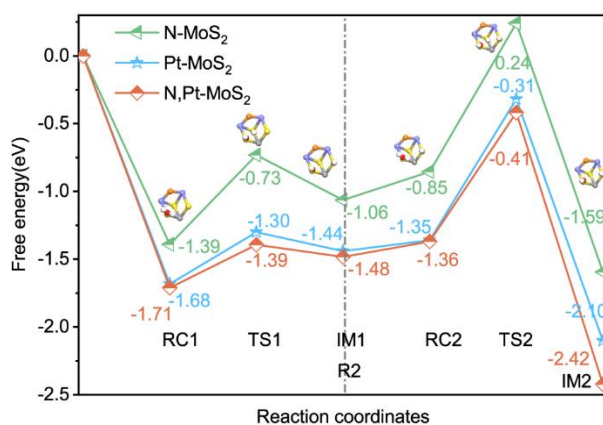

Figure S21. Zoom-in relative energy diagram along the reaction coordinate of N-MoS_2, Pt-MoS_2, and N,Pt-MoS_2 nanosheets.

Table S7. Integration areas of overlap part between S orbital and water molecule below Fermi level.

Sample	Area (number of states)
MoS_2	1.13
N-MoS_2	1.08
N,Pt-MoS_2	0.91

References

1 X. Chen, Z. Wang, Y. Wei, X. Zhang, Q. Zhang, L. Gu, L. Zhang, N. Yang and R. Yu, *Angew. Chem. Int. Ed.,* 2019, **58**, 17621-17624.

2 Q. Xiong, Y. Wang, P. F. Liu, L. R. Zheng, G. Wang, H. G. Yang, P. K. Wong, H. Zhang and H. Zhao, *Adv. Mater.*, 2018, **29,** 1801450.

3 T. Sun, J. Wang, X. Chi, Y. Lin, Z. Chen, X. Ling, C. Qiu, Y. Xu, L. Song, W. Chen and C. Su, *ACS Catal.*, 2018, **8**, 7585-7592.

4 Y. Feng, T. Zhang, J. Zhang, H. Fan, C. He and J. Song, *Small*, 2020, **16**, 2002850.

5 S. Park, C. Kim, S. O. Park, N. K. Oh, U. Kim, J. Lee, J. Seo, Y. Yang, H. Y. Lim, S. K. Kwak, G. Kim and H. Park, *Adv. Mater.*, 2020, **32**, 2001889.

6 Y. Guo, J. Tang, J. Henzie, B. Jiang, W. Xia, T. Chen, Y. Bando, Y. M. Kang, M. S. A. Hossain, Y. Sugahara and Y. Yamauchi, *ACS Nano*, 2020, **14**, 4141-4152.

7 P. Kuang, M. He, H. Zou, J. Yu and K. Fan, *Appl. Catal. B- Environ.*, 2019, **254**, 15-25.

8 D. Wang, Q. Li, C. Han, Z. Xing and X. Yang, *Appl. Catal. B- Environ.*, 2019, **249**, 91-97.

9 Y. Yang, H. Yao, Z. Yu, S. M. Islam, H. He, M. Yuan, Y. Yue, K. Xu, W. Hao, G. Sun, H. Li, S. Ma, P. Zapol and M. G. Kanatzidis, *J. Am. Chem. Soc.*, 2019, **141**, 10417-10430.

10 C. Zhang, Y. Cui, Y. Yang, L. Lu, S. Yu, Z. Meng, Y. Wu, Y. Li, Y. Wang, H. Tian and W. Zheng, *Adv. Funct. Mater.*, 2021, **31**, 2105372.

11 Z. Zhao, H. Liu, W. Gao, W. Xue, Z. Liu, J. Huang, X. Pan and Y. Huang, *J. Am. Chem. Soc.*, 2018, **140**, 9046-9050.

12 X. Yu, E. C. Dos Santos, J. White, G. Salazar-Alvarez, L. G. Pettersson, A. Cornell and M. Johnsson, *Small*, 2021, 2104288.

13 K. Rui, G. Zhao, M. Lao, P. Cui, X. Zheng, X. Zheng, J. Zhu, W. Huang, S. X. Dou and W. Sun, *Nano Lett.*, 2019, **19**, 8447-8453.

14 P. Wang, K. Jiang, G. Wang, J. Yao and X. Huang, *Angew. Chem. Int. Ed.*, 2016, **128**, 13051-13055.

15 M. Lao, K. Rui, G. Zhao, P. Cui, X. Zheng, S. X. Dou and W. Sun, *Angew. Chem. Int. Ed.*, 2019, **131**, 5486-5491.

16 X. Huang, Z. Zeng, S. Bao, M. Wang, X. Qi, Z. Fan and H. Zhang, *Nat. Commun.*, 2013, **4**, 1-8.

17 H. Zhang, P. An, W. Zhou, B. Y. Guan, P. Zhang, J. Dong and X. W. D. Lou, *Sci. Adv.*, 2018, **4**, 6657.

18 J. Park, S. Lee, H. E. Kim, A. Cho, S. Kim, Y. Ye, J. W. Han, H. Lee, J. H. Jang and J. Lee, *Angew. Chem. Int. Ed.*, 2019, **58**, 16038-16042.

19 J. Deng, H. Li, J. Xiao, Y. Tu, D. Deng, H. Yang, H. Tian, J. Li, P. Ren and X. Bao, *Energy Environ. Sci.*, 2015, **8**, 1594-1601.